Supplementary Information for

ICAM-1 orchestrates the abscopal effect of tumor radiotherapy

Yang Zhao[1†], Ting Zhang[1†], Yanpu Wang[1], Dehua Lu[1], Jinhong Du[1], Xun Feng[1], Haoyi Zhou[1], Ning Liu[1], Hua Zhu[2], Shangbin Qin[3], Chenxin Liu[1], Xianshu Gao[3], Zhi Yang[2], Zhaofei Liu[1, 4*]

[1]Medical Isotopes Research Center and Department of Radiation Medicine, School of Basic Medical Sciences, Peking University Health Science Center, Beijing 100191, China

[2]Key Laboratory of Carcinogenesis and Translational Research (Ministry of Education/Beijing), Department of Nuclear Medicine, Peking University Cancer Hospital & Institute, Beijing 100142, China

[3]Department of Radiation Oncology, Peking University First Hospital, Beijing100034, China

[4]State Key Laboratory of Natural and Biomimetic Drugs, Peking University, Beijing 100191, China.

[†]These authors contributed equally to this work.

*To whom correspondence should be addressed: Zhaofei Liu, Ph.D., Medical Isotopes Research Center, School of Basic Medical Sciences, Peking University Health Science Center, 38 Xueyuan Road, Beijing 100191, China. Email: liuzf@bjmu.edu.cn

This PDF file includes:

Supplementary Materials and Methods

Figures S1 to S28

Tables S1 to S2

SI References

Other supplementary material for this manuscript includes the following:

Dataset S1

Supplementary Materials and Methods

Cell culture and animal models

The 4T1 murine breast cancer and CT26 murine colon carcinoma cell lines were purchased from American Type Culture Collection (Manassas, VA), and the 4T1 cells stably transfected with firefly luciferase (4T1-fLuc) was generated as previously described (1). All tumor cells were cultured in RPMI-1640 medium (Invitrogen, Carlsbad, CA). Human embryonic kidney HEK 293T cells were kindly provided by Dr. Tao Xu (Institute of Biophysics, China Academy of Science), and were cultured in Dulbecco modified Eagle medium (DMEM). All cells were grown in medium supplemented with 10% fetal bovine serum (FBS) at 37°C in a humidified atmosphere containing 5% CO_2.

All animal experiments were carried out according to protocols approved by the Institutional Animal Care and Use Committee at Peking University. Transgenic OT-I mice and ICAM-1-knockout mice (5–6 weeks of age) were purchased from Shanghai Model Organisms Center, Inc. (Shanghai, China). The ICAM-1-knockout mice were established using a CRISPR/Cas9-mediated genome-editing system. After co-injection of the guide RNA and Cas9 mRNA into fertilized eggs of C57BL/6 mice, mutant lines with a 310-base-pair deletion were generated. The founders were then genotyped by PCR, followed by DNA sequencing analysis for confirmation. Female BALB/c mice (5-6 weeks of age) were purchased from the Department of Laboratory Animal Science of Peking University (Beijing, China). To establish the 4T1 or CT26 tumor-bearing mouse model, 1×10^6 tumor cells were injected subcutaneously into the right flanks of BALB/c mice. For the bilateral tumor-bearing mouse model, mice were injected subcutaneously with 1×10^6 tumor cells in the right flank and 2×10^5 cells in the left flank. Tumor growth was measured using a caliper and tumor volume was calculated as

volume = length × width^2/2. For the establishment of the dual subcutaneous and lung metastatic tumor model, 1 × 10^6 4T1-fLuc tumor cells were inoculated subcutaneously into the right flanks of mice and 1 × 10^5 4T1-fLuc tumor cells were injected 3 days later into the mice through the tail vein to form a metastatic lung tumor mimic.

Radiation treatment

The bilateral 4T1 or CT26 tumor-bearing mice with right tumor volumes of approximately 100 mm^3 and left tumor volumes of approximately 50 mm^3 were divided randomly into the RT and control groups. For the RT groups, the right tumors were locally irradiated using an X-ray irradiator (RS2000 PRO, 160 kV, 25 mA; Rad Source Technologies, Suwanee, GA) at a dose rate of 4.12 Gy/min. The irradiation was delivered to a field including the tumor, with 5-mm margins, and the tumors were irradiated with a total dose of 24 Gy (three fractions of 8 Gy administered every other day). On day 7, the mice in the RT group were divided into two groups: the responder and nonresponder groups. The responder group comprised of mice with a <50% change in the volume of nonirradiated tumor between days 0 and 7 [$(V_7–V_0)/V_0 \times 100\% < 50\%$]. Mice with a >50% change in the volume of nonirradiated tumor between days 0 and 7 [$(V_7–V_0)/V_0 \times 100\% > 50\%$) were allocated to the nonresponder group (Fig. 1A). Mice were then euthanized, and tumor tissues were harvested for subsequent proteomics analysis, western blotting, immunofluorescence staining, and flow cytometric analyses.

Proteomics analysis

Proteomics analysis was performed as described previously (2). Briefly, tumor tissues were harvested and proteins were extracted. Proteins were then incubated with trypsin (protein-to-enzyme ratio = 50:1) overnight at 37°C, and the released peptides

were collected by centrifugation. High-pH reverse-phase chromatography was used for peptide separation, and elution was monitored with an ultraviolet-visible detector at 214 nm. After vacuum drying, the eluted peptides were subjected to liquid chromatography tandem-mass spectrometry analysis. The UniProt human protein database was used for protein identification, and the data were analyzed using the MaxQuant software package (version 1.4.1.2). The minimum ratio count for label-free quantitation was set as 2, and the match-between-runs option was enabled. Upregulated or downregulated proteins were defined as those with a significant change in the protein ratio (P <0.05). The significance of the P value was calculated using the Perseus computational platform (version 1.4.1.3).

Western blotting

Tumor tissues were homogenized, and proteins were extracted using radioimmunoprecipitation assay buffer. Protein concentrations were determined using a BCA assay kit (Thermo Fisher Scientific, Waltham, MA). After protein separation using sodium dodecyl sulfate-polyacrylamide gel electrophoresis (SDS-PAGE), the proteins were transferred to a polyvinylidene difluoride membrane and blocked in 5% skimmed milk for 1 h. The membrane was incubated overnight at 4°C with anti-ICAM-1 primary antibody (1:200; Santa Cruz, CA), followed by incubation with DyLight549-conjugated secondary antibodies (1:1000; EarthOx, Millbrae, CA) for 1 h at room temperature, and it was imaged using the Molecular Imager PharosFX™ Plus System (Bio-Rad Laboratories, Hercules, CA).

Preparation of ICAM-1-targeted imaging probes

The ICAM-1-specific near-infrared fluorescence (NIRF) and positron emission

tomography (PET) imaging probes were synthesized using previously described methods (3, 4). Briefly, anti-ICAM-1 antibody (αICAM-1; clone YN1/1.7.4; BioXcell, West Lebanon, NH) was digested using a Fab preparation kit (Thermo Fisher Scientific), and then the Fab fragment of αICAM-1 (αICAM-1/Fab) was obtained.

To synthesize the NIRF imaging probe, αICAM-1/Fab was mixed with DyLight800-NHS ester (Thermo Fisher Scientific) at a molar ratio of 1:10 in $NaHCO_3$ buffer (pH 8.4). After an overnight reaction at 4°C, the DyLight800-labeled αICAM-1/Fab was purified using a PD-10 desalting column (GE Healthcare, Piscataway, NJ). The purity of Dye-αICAM-1/Fab was confirmed by SDS-PAGE, and optical imaging was performed using the Maestro In-Vivo Imaging System (CRI, Woburn, MA). The isotype-matched control probe (Dye-IgG/Fab) was also prepared using the same protocol.

To synthesize ^{64}Cu-labeled αICAM-1/Fab, αICAM-1/Fab was first conjugated with the bifunctional chelator *p*-SCN-Bn-NOTA (Macrocyclics, Dallas, TX) at a molar ratio of 1:10 in $NaHCO_3$ buffer (pH 8.4). NOTA-αICAM-1/Fab was then purified using a PD-10 desalting column. For radiolabeling, 74 MBq $^{64}CuCl_2$ was added to 40 μg of NOTA-αICAM-1/Fab in sodium acetate buffer (pH 5.4). After shaking for 40 min at 37°C, ^{64}Cu-NOTA-αICAM-1/Fab was purified using a PD-10 desalting column. The purity of ^{64}Cu-NOTA-αICAM-1/Fab was confirmed by instant thin-layer chromatography, and the ICAM-1 binding specificity of ^{64}Cu-NOTA-αICAM-1/Fab was determined using a cell binding assay. The isotype-matched control probe (^{64}Cu-NOTA-IgG/Fab) was prepared using the same protocol.

In vivo small-animal NIRF and PET imaging

For *in vivo* NIRF imaging, each tumor-bearing mouse was injected intravenously

with 0.5 nmol of Dye-αICAM-1/Fab or Dye-IgG/Fab. Optical imaging was performed using the Maestro *in vivo* Imaging System (CRI) at 2, 6, and 24 h postinjection (p.i.). The excitation wavelength of the imaging was 770 nm and the emission wavelength was 794 nm. The region of interest (ROI) for each tumor was drawn using Maestro 2.4 software (Bio-Rad).

For *in vivo* small-animal PET imaging, 18.5 MBq ^{64}Cu-NOTA-αICAM-1/Fab or a control probe (^{64}Cu-NOTA-IgG/Fab) was administered to each tumor-bearing mouse intravenously. At 2, 6, and 24 h p.i., 10-min static PET scanning was performed using a Super Nova PET/CT scanner (Pingseng Healthcare, Kunshan, China). PET images were analyzed, and the ROI-derived percentage of the injected dose per gram of tissue (%ID/g) values was calculated as described previously (5).

Upregulation of ICAM-1 by adenovirus

The recombinant adenovirus-expressing mouse ICAM-1 (ICAM-1 Ad) and the control adenovirus (control Ad) were custom made by ViGene Biosciences (Jinan, China). HEK293T was used for *in vitro* transfection according to the manufacturer's instructions, and flow cytometric analysis was performed to verify the expression of ICAM-1.

To investigate the effect of the combination therapy of RT and ICAM-1 Ad, the 4T1 tumor-bearing mice were randomly divided into two groups (n = 14–15 per group): (i) RT + control Ad and (ii) RT + ICAM-1 Ad. For the adenovirus injection, 25 μL ICAM-1 Ad or control Ad (10^8 PFUs/mouse) in phosphate-buffered saline (PBS) was injected into the tumors on day 0, 3, and 6, respectively. X-ray RT of the tumor was performed on day 3, 5, and 7. On day 10, five mice from each of the RT + control Ad and RT + ICAM-1 Ad groups were euthanized, and their tumor tissues were harvested for flow

cytometric analysis of $CD8^+$ and $CD4^+$ T cells.

To investigate the role of ICAM-1 in the abscopal effect induced by radiotherapy (RT), the bilateral 4T1 tumor-bearing mice were divided randomly into 5 groups (n = 6–14 per group) and were treated as follows: (i) PBS, (ii) ICAM-1 Ad, (iii) RT + PBS, (iv) RT + control Ad, or (v) RT + ICAM-1 Ad. For the adenovirus injection, 25 μL ICAM-1 Ad or control Ad (10^8 PFUs/mouse) in PBS was injected into the left tumors (nonirradiated tumors) on days 0, 3, and 6, respectively. X-ray RT was irradiated on days 3, 5, and 7 to the right tumor. On day 10, five mice from each of the RT + control Ad and RT + ICAM-1 Ad groups were euthanized, and their tumor tissues were harvested for flow cytometric analysis and immunofluorescence staining.

ICAM-1 knockdown and T cell killing assay

Lentiviruses carrying shRNA-targeting mouse ICAM-1 lentiviral vectors (GV493) were obtained from JiKai Gene (Shanghai, China). The shRNA sequence was as follows: 5′-AGATCAGGATATACAAGTTAC-3′. OT-I $CD8^+$ T cells were derived from transgenic OT-I mice, and knockdown of ICAM-1 in the OT-I $CD8^+$ T cells was performed according to the procedure provided by JiKai Gene with slight modifications. The viruses were used to infect cells in the presence of protamine (Sigma-Aldrich, St. Louis, MO). Forty-eight hours later, the knockdown of ICAM-1 was identified and verified by flow cytometric analysis.

For the T cell killing assay, wild-type $CD8^+$ T cells or ICAM-1 knockdown OT-I $CD8^+$ T cells [specifically recognizing ovalbumin (OVA)] were added to pre-seeded B16-OVA cells at a 1:1 ratio in the T cell culture medium with interleukin-2 (100 IU/mL). After coculturing for 2 days, the apoptosis of tumor cells was detected using an Annexin V-FITC Apoptosis Detection Kit (Solarbio, Beijing, China). Flow

cytometric analysis of IFNγ and CD107a was also conducted to evaluate the activation of $CD8^+$ T cells.

Synthesis of PLGA-IMQ nanoparticles

PEG-grafted PLGA co-polymer (PEG-PLGA; 50:50 (w/w), Mw ~5,000:10,000 Da) was purchased from Ruixi Biological Technology Co., Ltd (Xi-an, China). Imiquimod (IMQ; Sigma-Aldrich) was dissolved in DMSO at 2.5 mg/mL and then added to 10 mg/mL of PEG-PLGA dissolved in acetone. The ratio of IMQ to polymer was 1:5 (w/w). Experiments proved that the optimum concentration of IMQ was 400 μg/mL in the final water phase. Then, 1 mL of the mixture was dropped carefully into a 5 mL 2.5% w/v solution of polyvinyl alcohol (Sigma-Aldrich). After 1 h stirring and 12 h standing for organic phase evaporation, PLGA-IMQ nanoparticles were purified after centrifugation at 30,000 g for 5 min to remove unloaded IMQ.

The morphology and structure of PLGA-IMQ were characterized using a JEM-1400 transmission electron microscope (JEOL, Japan), and the particle size distribution and Zeta potential were measured by dynamic light scattering (Brookhaven Instruments, Holtsville, NY). The encapsulation efficiency of IMQ and the drug release ratio were determined using high-performance liquid chromatography (HPLC) with an ultraviolet-visible detector at 325 nm.

Toxicity studies of PLGA-IMQ

The 4T1 mouse tumor cells and RAW 264.7 mouse macrophages were cultured in RPMI-1640 medium. CTLL-2 mouse T lymphocytes were cultured in RPMI-1640 medium supplemented with interleukin-2 (100 IU/mL). The cytotoxicity of PLGA-IMQ was evaluated in these cell lines using Cell Counting Kit-8 (CCK8, Dojindo

Laboratories, Kumamoto, Japan) assay. Briefly, cells were seeded in a 96-well flat-bottom plate at a density of 5×10^3 cells /100 μL per well and incubated with PLGA-IMQ (720 μg IMQ equivalent/mL) for 48 h. Then, the cell medium was refreshed and 10 μL of CCK8 solution was added to each well for incubation at 37°C for an additional 2 h. Finally, the absorbance of each well was measured at 450 nm.

For *in vivo* toxicity study, the treatment dose of PLGA-IMQ was injected intravenously into the BALB/c mice. After 12 days, 20 μL of blood was collected into anticoagulant fluid for routine blood analysis. Meanwhile, the major organs (including the heart, liver, spleen, lung, and kidney) were collected for hematoxylin & eosin staining analysis.

***In vivo* combination therapy**

To study the combined effect of IMQ and RT, bilateral 4T1 or CT26 tumor-bearing mice were divided randomly into 6 groups (n = 6–15 per group): (i) PBS, (ii) IMQ, (iii) RT + PBS, (iv) RT + IMQ, (v) RT + anti-ICAM-1 blocking antibody, or (vi) RT + IMQ + ICAM-1 blocking antibody. For IMQ treatment groups, 20 μg of IMQ in PBS was injected intratumorally into the left tumor daily from days 0 to 7. For the ICAM-1 blocking group, 50 μg of anti-ICAM-1 antibody (clone YN1/1.7.4; BioXcell) was injected intratumorally into the left tumor on days 1, 3, 5, and 7. The right tumor of each mouse was irradiated thrice with a total dose of 24 Gy (8 Gy on days 3, 5, and 7). On day 12, three mice from each group of the RT + PBS and RT + IMQ groups were euthanized, and their tumors were harvested for western blotting and flow cytometric analysis.

To study the combined effect of PLGA-IMQ and RT, bilateral 4T1 tumor-bearing mice were divided randomly into 4 groups (n = 8 per group): (i) PBS control, (ii) PLGA-

IMQ, (iii) RT + PBS, and (iv) RT + PLGA-IMQ. To explore the combined effect of PLGA-IMQ and RT in the dual subcutaneous and lung metastatic tumor model, mice were randomly divided into two groups (n = 7–8 per group): (i) RT + PBS and (ii) RT + PLGA-IMQ. For the PLGA-IMQ treatment, each mouse was injected intravenously with PLGA-IMQ (720 μg IMQ equivalent) in PBS on day 0. For RT, the right tumors of the bilateral 4T1 tumor-bearing mouse model or the subcutaneous tumors of the dual subcutaneous and lung metastatic tumor model were irradiated thrice with a total dose of 24 Gy (8 Gy on days 0, 2, and 4).

In vivo blocking studies

For the *in vivo* blocking of ICAM-1, 50 μg of anti-ICAM-1 antibody (clone YN1/1.7.4; BioXcell) was injected intratumorally into the indicated tumors every other day for 4 days. For the *in vivo* depletion of the $CD4^+$ or $CD8^+$ T cells, 50 μg of anti-CD8 antibody (clone YTS 169.4; BioXcell) or anti-CD4 antibody (clone GK1.5; BioXcell) was injected intravenously every other day for 4 days.

Bioluminescence imaging (BLI) of lung metastasis

Longitudinal BLI was performed to evaluate the growth of the lung metastatic lesions. BLI was performed using the IVIS spectrum system (Xenogen, Alameda, CA) 10 min after D-luciferin administration. The BLI signal intensity was quantified as the sum of all detected photon counts within the region of interest after subtracting background luminescence.

Flow cytometric analysis

Tumor tissues were harvested from the mice and then digested into single-cell

suspensions. The single-cell suspensions of the tumor tissues were stained using fluorescently labeled antibodies (*SI Appendix*, Table S2) for different markers: anti-CD11a, anti-CD11b, anti-CD11c, anti-CD3, anti-CD4, anti-CD8, anti-ICAM-1, anti-CD31, anti-CD19, anti-CD45, anti-NK1.1, anti-IFNγ, and anti-FoxP3. FITC-labeled anti-ICAM-1 was prepared in-house by conjugating anti-ICAM-1 antibody (BioXcell) with FITC-NHS (Pierce) using a previously described method (6). For intracellular cytokine staining, the cells were treated with BD Cytofix/Cytoperm Plus (with GolgiPlug; BD Pharmingen) according to the manufacturer's instructions. All the samples were analyzed using the FACS Calibur flow cytometer (Becton Dickinson, San Jose, CA).

For the experiment regarding tumor-associated antigen (TAA) stimulation, single-cell suspensions of the spleen were obtained and stimulated with TAA (proteins obtained from tumor tissues) for 12 h at 37°C. They were then stained with fluorescently labeled anti-CD45, anti-CD8, anti-ICAM-1, and anti-IFNγ for direct analysis. For the experiment regarding immune synapse formation, splenocytes from wild-type or ICAM-1 knockout mice were stained with fluorescently labeled anti-CD3, anti-CD8, anti-MHCII, and anti-CD11c. The cells were then sorted into $CD8^+$ T cells ($CD3^+CD8^+$) and dendritic cells ($MHCII^+CD11c^+$) using the Aria Sorp flow cytometer (Becton Dickinson). Dendritic cells and $CD8^+$ T cells were treated with TAA and anti-ICAM-1 antibody, respectively, for 30 min. Then, the two types of cells were cocultured for 30 min at 37°C and stained with fluorescently labeled anti-IFNγ and anti-CD107a. All the samples were then analyzed using a FACS Gallios flow cytometer (Beckman Coulter, San Jose, CA). To directly visualize the formation of immune synapses, $CD8^+$ T cells and dendritic cells were stained with the cell trackers CM-Dil and CMDFA (Invitrogen), respectively. After coculture, they were visualized under a confocal

microscope (Leica, Wetzlar, Germany).

Immunofluorescence staining

Frozen 4T1 tumor sections were fixed with ice-cold acetone and blocked with 5% bovine serum albumin (in PBS). The sections were then incubated with primary antibodies for 2 h at room temperature and then incubated with DyLight549- or FITC-conjugated secondary antibodies (1:200; EarthOx) for 1 h. After washing, tumor sections were visualized under a confocal microscope (Leica). The primary antibodies that were used included anti-ICAM-1 (1:100; Santa Cruz), anti-CD8 (1:100; BioXcell), anti-Ki67 (1:250; Abcam, Cambridge, MA), and anti-CD31 (1:100; BD Biosciences, San Jose, CA). The quantification of fluorescence intensity was determined using ImageJ software (NIH, Bethesda, MD).

Immunohistochemical staining of patient samples

Patient tumor samples before and after RT were obtained from Peking University First Hospital, and were de-identified prior to their use in this study. Written informed consent was obtained from all patients and all the procedures were approved by the Institutional Review Board of Pekin University First Hospital. Information regarding RT doses, RT time-points, and sample collection time-points is described in Supplementary Table S1. For human ICAM-1 staining, paraffin-embedded tumor tissues were deparaffinized, the endogenous peroxidase activity was abolished using hydrogen peroxide, and the antigen was retrieved. Tumor sections were then incubated with antihuman ICAM-1 antibody (1:200; Abcam) overnight at 4°C. Tumor sections were then incubated with a horseradish peroxidase–conjugated secondary antibody for 2 h and visualized by incubation with the diaminobenzidine substrate. After staining,

the slides were visualized using a Leica DM5000B microscope (Leica), and the intensity of ICAM-1 was quantified using ImageJ software (NIH).

Statistical analyses

Statistical analyses were performed using GraphPad Prism Version 7.0 software (GraphPad Software, San Diego, CA). Quantitative data are presented as mean ± standard deviation (SD). Comparisons of two groups were performed using a two-tailed unpaired Student *t* test. Comparisons of patients' immunohistochemical staining results before and after radiotherapy were performed using a two-tailed paired Student *t* test. Comparisons of multiple groups were performed by using one-way analysis of variance (ANOVA) with a post-hoc Tukey test. Tumor growth curves over time were compared by two-way ANOVA. Standard Pearson correlation analysis was used for determining the correlation between two variables. *P* values of <0.05 were considered statistically significant.

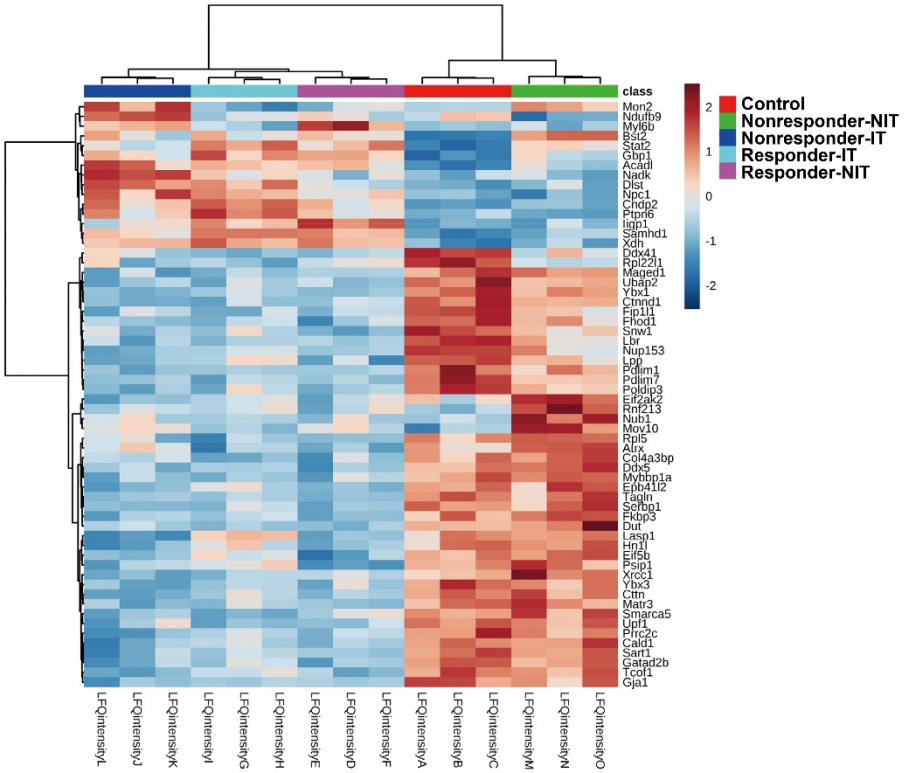

Figure S1. Heat map of expression levels of the top 60 altered proteins. The red color indicates high abundance and blue color indicates low abundance.

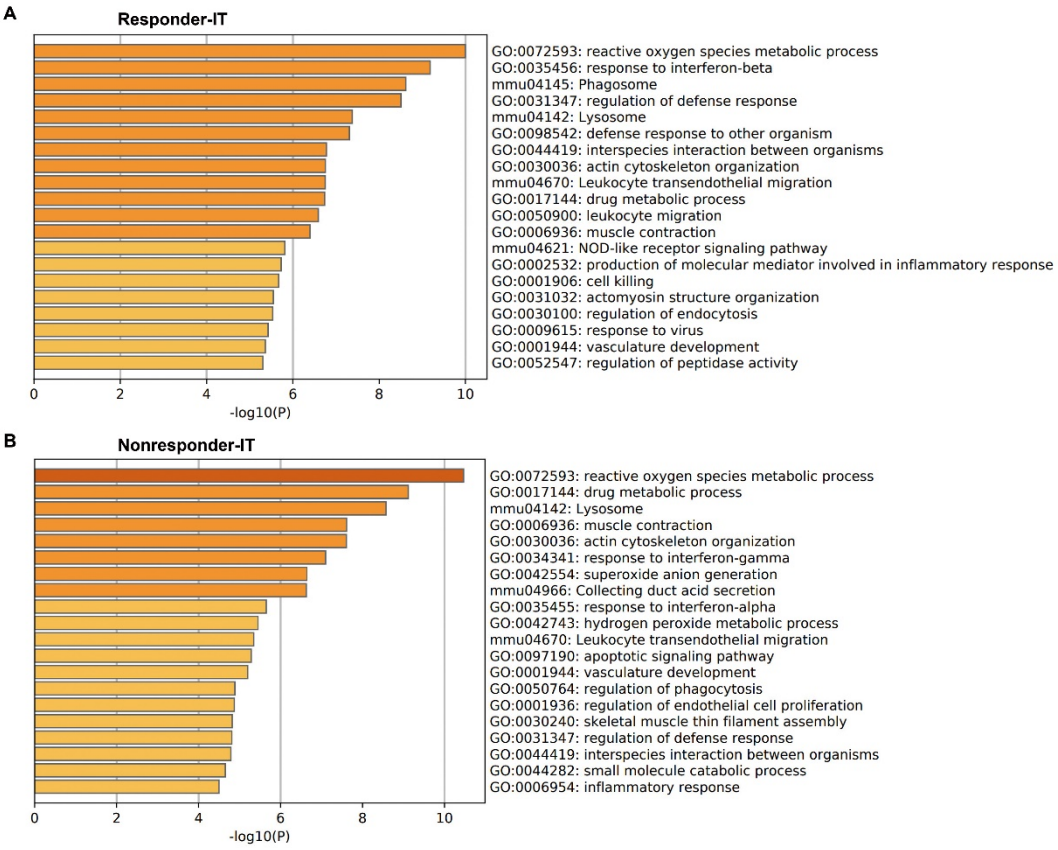

Figure S2. Enrichment pathway analysis of the radiotherapy (RT)-regulated proteins in irradiated tumors. (A–B) Proteins (fold-change >2.5, adjusted P <0.01) in the irradiated tumors of the responder group (responder-IT) (A) and irradiated tumors in the nonresponder group (nonresponder-IT) (B) were analyzed. The color gradient of the bar graph shows the -$\log_{10}$ (adjusted P value) of each associated pathway; darker orange colors indicate lower P values.

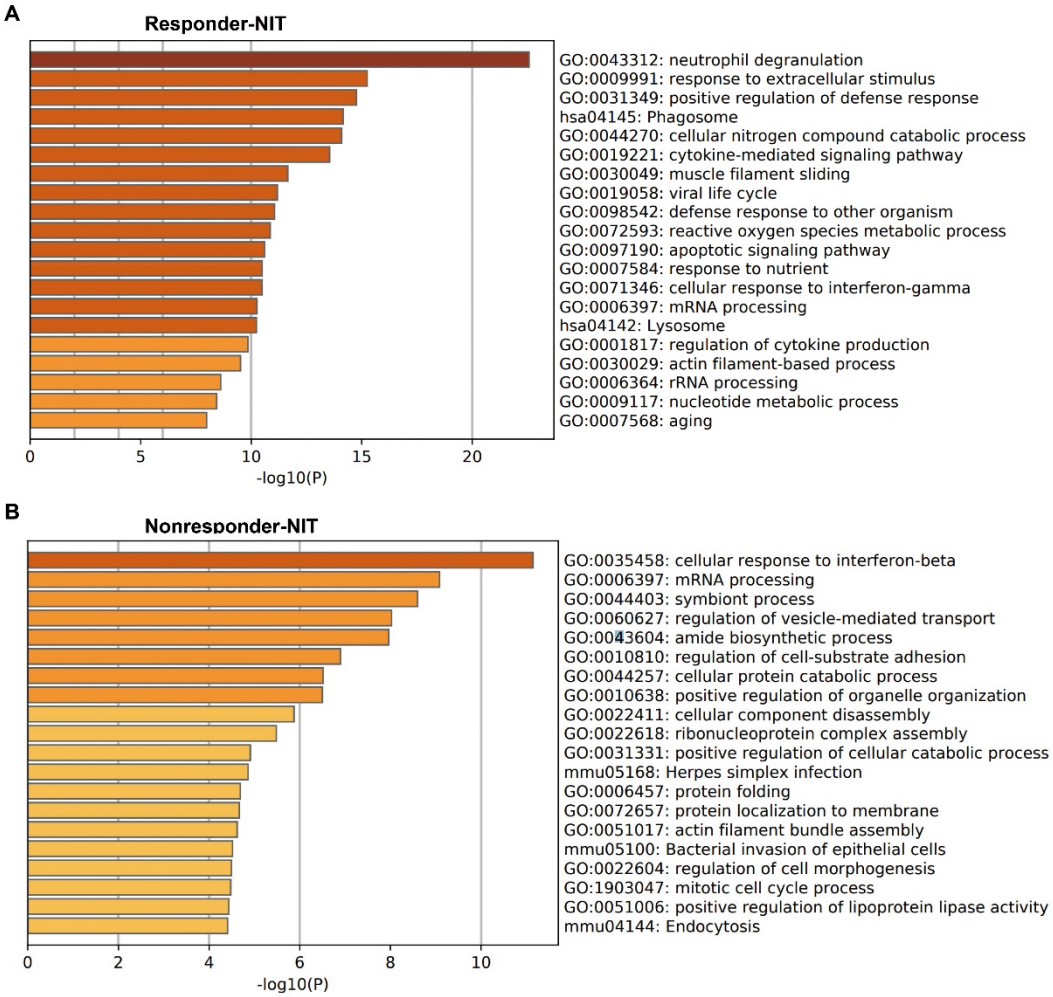

Figure S3. Enrichment pathway analysis of radiotherapy (RT)-regulated proteins in nonirradiated tumors. (A–B) Proteins (fold-change >2.5, adjusted *P* <0.01) in the nonirradiated tumors of the responder group (responder-NIT) (A) and nonirradiated tumors of the nonresponder group (nonresponder-NIT) (B) were analyzed. The color gradient of the bar graph shows the -$\log_{10}$ (adjusted *P* value) of each associated pathway; darker orange colors indicate lower *P* values.

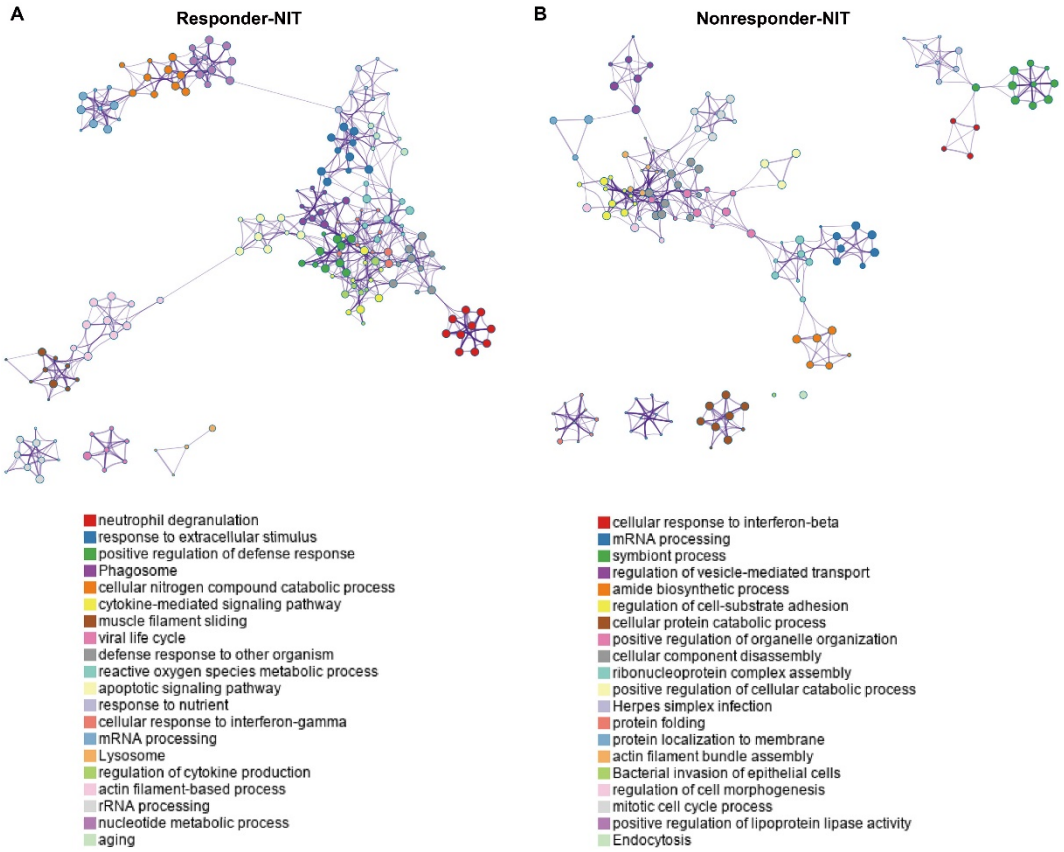

Figure S4. Regulated enrichment pathway network in nonirradiated tumors. (A–B) Nonirradiated tumors in the responder group (responder-NIT) (A) and nonirradiated tumors in the nonresponder group (nonresponder-NIT) (B) (fold-change >2.5, adjusted P <0.01) were analyzed. A node represents each enriched gene set of the indicated pathways from the molecular signature database.

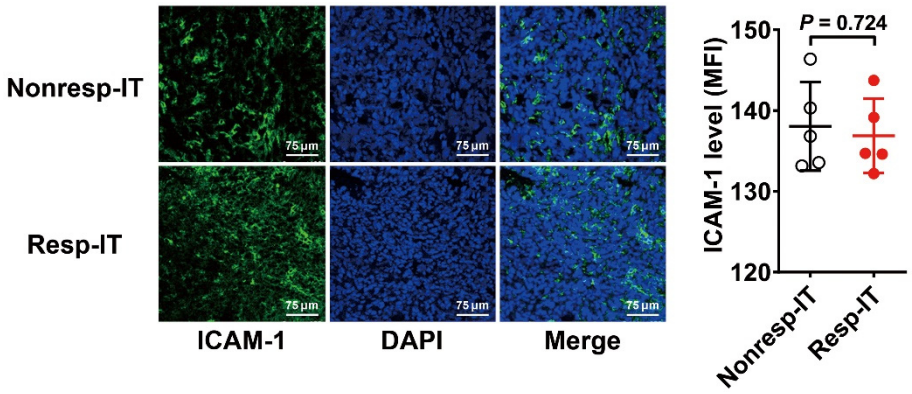

Figure S5. Immunofluorescence staining and quantitative analysis of ICAM-1 expression in the irradiated tumor tissues of the nonresponder group (nonresp-IT) and responder group (resp-IT). Data are presented as mean ± SD, n = 5. $P = 0.724$; by unpaired Student *t* test.

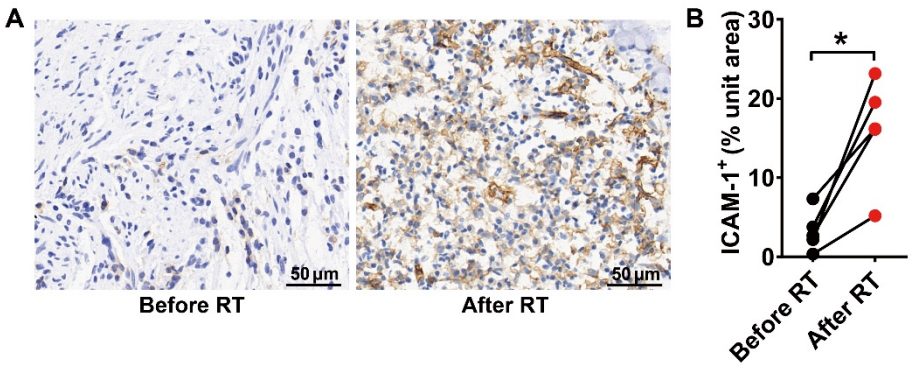

Figure S6. Immunohistochemical staining of ICAM-1 expression in human samples. (A–B) Representative immunohistochemical staining images (A) and quantitative results (B) in the tumor tissues before and after radiotherapy (RT) in cancer patients. Data are presented as mean ± SD, n = 5. *, P <0.05; by paired Student t test.

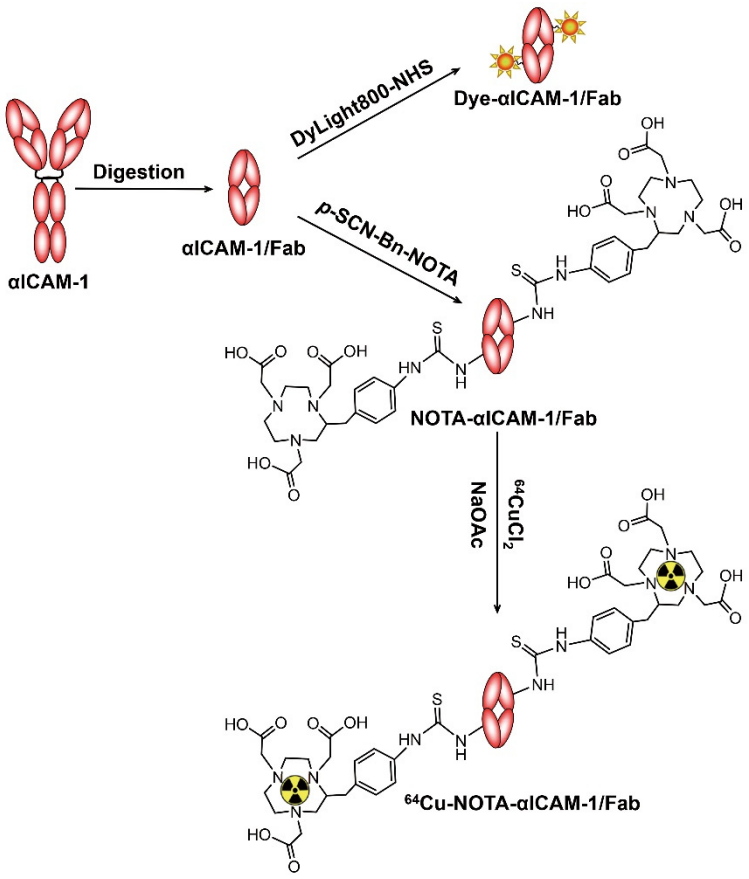

Figure S7. Synthetic scheme of Dye-αICAM-1/Fab and ^{64}Cu-NOTA-αICAM-1/Fab. Dye-αICAM-1/Fab was synthesized by directly coupling the Fab fragment of αICAM-1 (αICAM-1/Fab) with DyLight800-NHS. ^{64}Cu-NOTA-αICAM-1/Fab was prepared by radiolabeling NOTA-conjugated αICAM-1/Fab with $^{64}CuCl_2$.

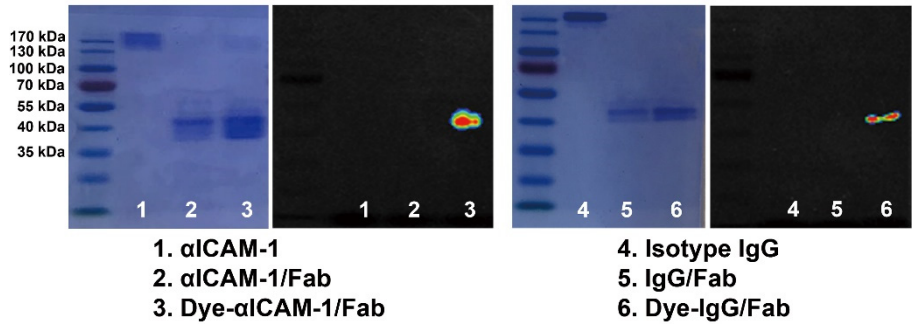

Figure S8. Purification analysis of Dye-αICAM-1/Fab and Dye-IgG/Fab. Sodium dodecyl sulfate-polyacrylamide gel electrophoresis (SDS-PAGE) and near-infrared fluorescence images of the anti-ICAM-1 antibody (αICAM-1), the Fab fragment of αICAM-1 (αICAM-1/Fab), DyLight800-conjugated αICAM-1/Fab (Dye-αICAM-1/Fab), and isotype control IgG, IgG/Fab, and Dye-IgG/Fab.

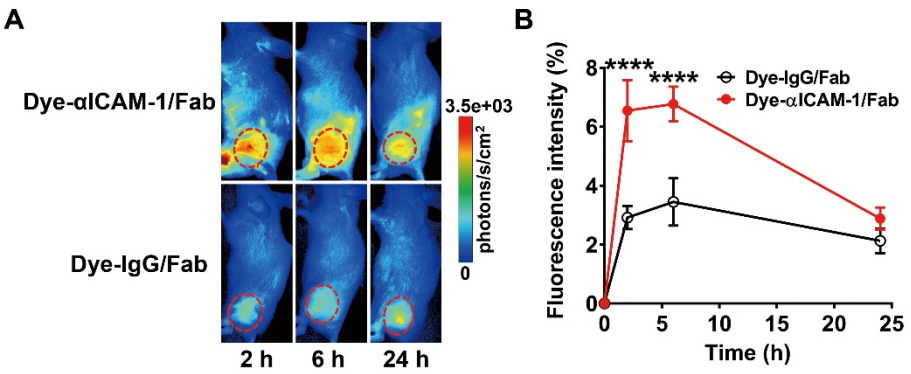

Figure S9. *In vivo* specific targeting of Dye-αICAM-1-Fab. (A–B) Representative near-infrared fluorescence images (A) and quantitative analysis of tumor uptake (B) of Dye-αICAM-1-Fab or Dye-IgG-Fab in 4T1 tumor-bearing mice at 2, 6, and 24 h p.i. Tumors are indicated by red circles. Data are presented as mean ± SD, n = 5. ****, P <0.0001; by unpaired Student t test.

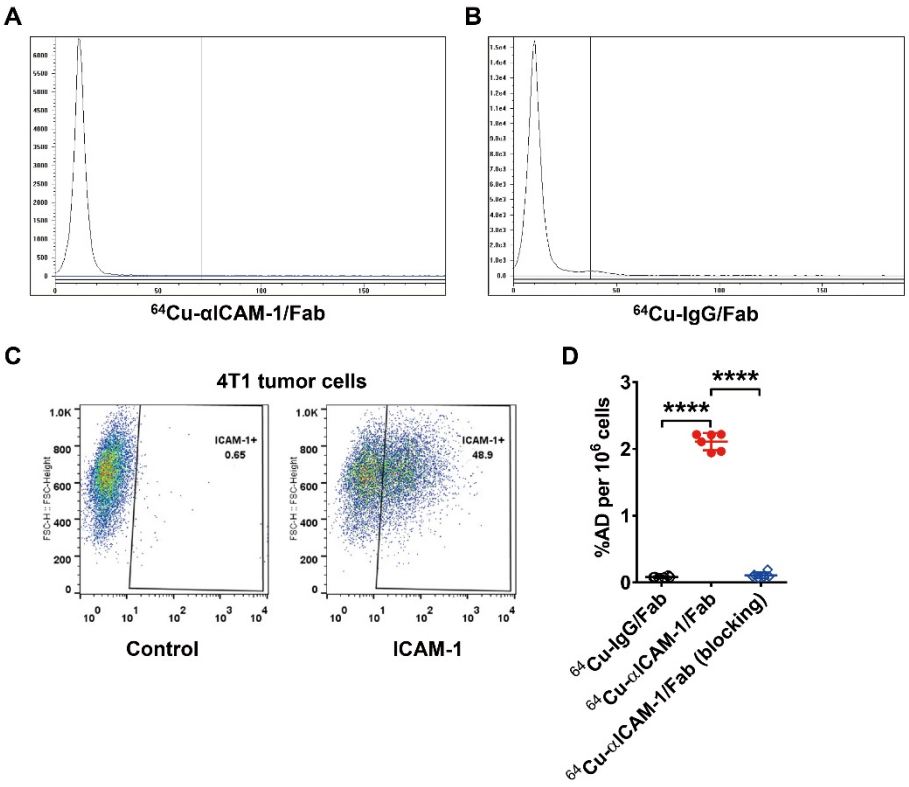

Figure S10. Characterization of ^{64}Cu-NOTA-αICAM-1/Fab. (A–B) Purification analysis of ^{64}Cu-NOTA-αICAM-1/Fab (^{64}Cu-αICAM-1/Fab) and ^{64}Cu-NOTA-IgG/Fab (^{64}Cu-IgG/Fab). High purity of ^{64}Cu-αICAM-1/Fab (A) and ^{64}Cu-IgG/Fab (B) was confirmed by instant thin-layer chromatography. (C) Representative flow cytometry plots showing positive-ICAM-1 expression on 4T1 tumor cells. (D) Cell binding assay of ^{64}Cu-αICAM-1/Fab and ^{64}Cu-IgG/Fab on 4T1 tumor cells with or without the blocking of an anti-ICAM-1 antibody. Data are presented as mean percentage added dose per million cells (%AD/10^6 cells) ± SD, n = 6. ****, P <0.0001; by 1-way ANOVA with a Tukey post-hoc test.

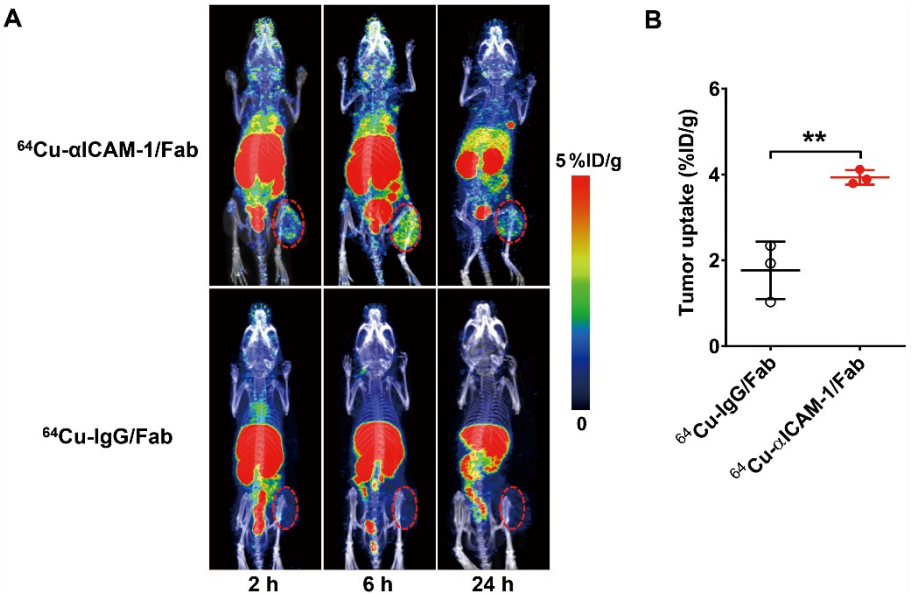

Figure S11. *In vivo* specific targeting of ^{64}Cu-NOTA-αICAM-1/Fab. (A) Representative small-animal positron emission tomography (PET)/CT images of ^{64}Cu-NOTA-αICAM-1/Fab (^{64}Cu-αICAM-1/Fab) or ^{64}Cu-NOTA-IgG/Fab (^{64}Cu-IgG/Fab) at 2, 6, and 24 h p.i. in 4T1 tumor-bearing mice. Tumors are indicated by red circles. (B) Quantified tumor uptake of ^{64}Cu-αICAM-1/Fab and ^{64}Cu-IgG/Fab at 6 h p.i. Data are presented as mean ± SD, n = 3. **, P <0.01; by unpaired Student t test.

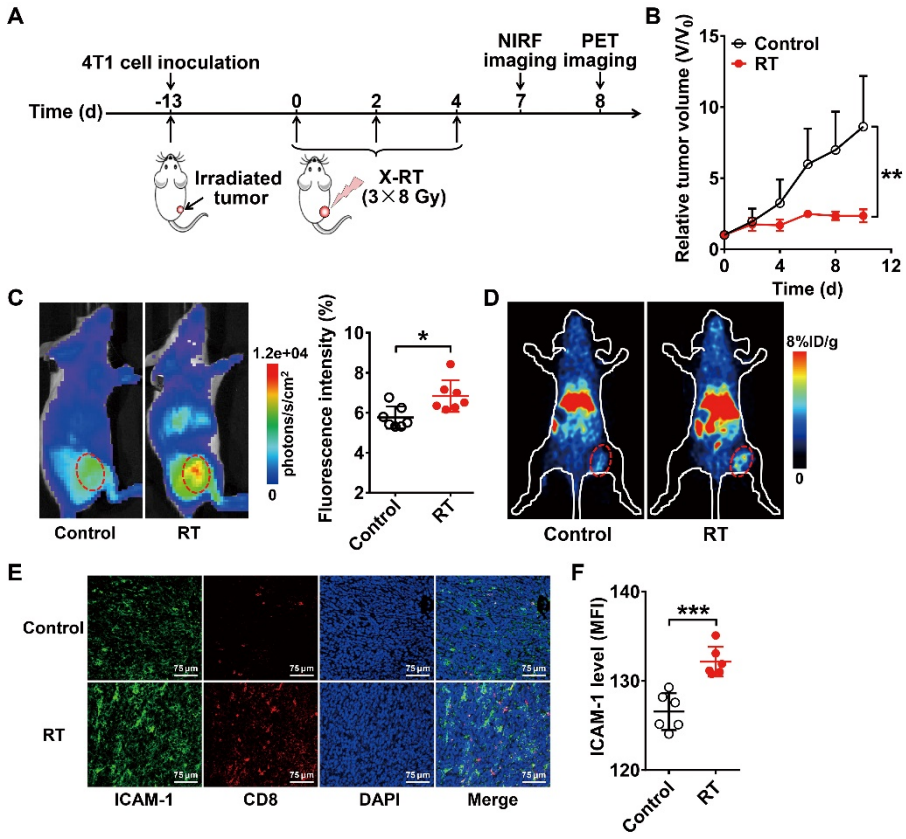

Figure S12. Effect of radiotherapy (RT) on the ICAM-1 expression of irradiated tumors. (A) Schedule of X-RT and *in vivo* imaging using Dye-αICAM-1/Fab or ^{64}Cu-NOTA-αICAM-1/Fab in the 4T1 tumor-bearing mouse model. (B)Tumor growth curves of 4T1 tumors after treatment with PBS or RT (n = 6–7 per group). (C) Representative *in vivo* near-infrared fluorescence images and quantitative analysis of tumor uptake of Dye-αICAM-1/Fab at 6 h p.i. in mice (n = 7 per group). (D) Representative small-animal PET images of ^{64}Cu-NOTA-αICAM-1/Fab at 6 h p.i. in mice. Tumors are indicated by red circles. (E–F) Representative immunofluorescence images (E) and quantitative analysis (F) of ICAM-1 expression in mice on day 12 (n = 6 per group). All the numerical data are presented as mean ± SD. *, P <0.05; **, P <0.01; ***, P <0.001; by 2-way ANOVA (B), or by unpaired Student t test (C and F).

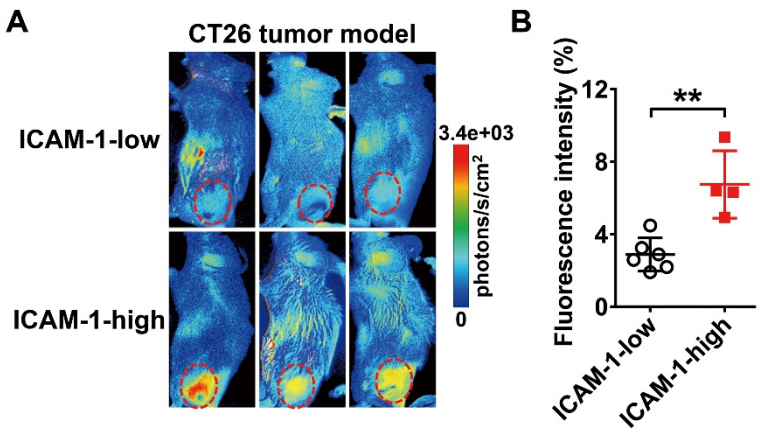

Figure S13. *In vivo* near-infrared fluorescence imaging of Dye-αICAM-1/Fab in the CT26 tumor model. (A–B) Representative *in vivo* near-infrared fluorescence images (A) and quantitative analysis (B) of tumor uptake of Dye-αICAM-1/Fab at 6 h p.i. in mice on day 7. High (n = 4) or low (n = 6) expression of ICAM-1 was differentiated by quantitative fluorescence intensity. Tumors are indicated by red circles. Data are presented as mean ± SD. **, P <0.01; by unpaired Student t test.

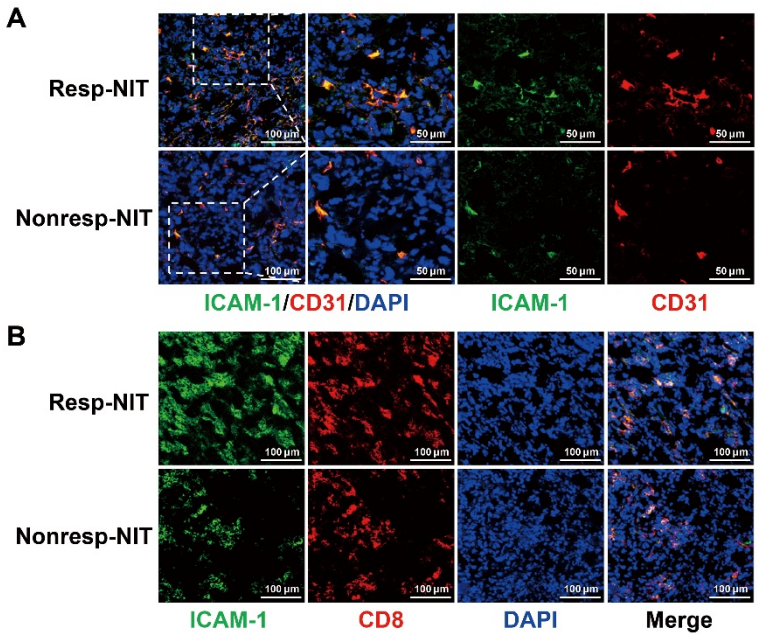

Figure S14. Overlay staining of ICAM-1 with CD31 and CD8 in 4T1 tumor tissues. (A–B) Immunofluorescence analysis of the colocalization of ICAM-1 with CD31 (to detect endothelial cells) (A) and CD8 (to detect $CD8^+$ T cells) (B) in 4T1 tumor tissues derived from nonirradiated tumors in the responder group (resp-NIT) or nonirradiated tumors in the nonresponder group (nonresp-NIT).

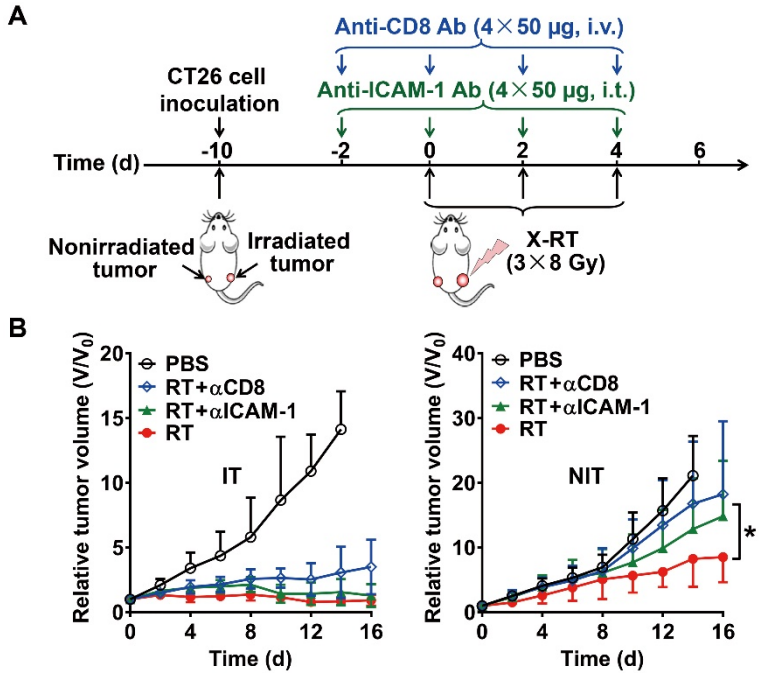

Figure S15. Radiotherapy (RT) treatment with *in vivo* anti-CD8 or anti-ICAM-1 blockade in CT26 tumor model. (A) Schematic illustration of RT in combination with anti-ICAM-1 blocking or anti-CD8 blocking. (B) Tumor growth curves of irradiated tumors (IT) and nonirradiated tumors (NIT) in CT26 tumor-bearing mice after the indicated treatments: control (PBS), RT alone, RT plus anti-ICAM-1 blocking (RT + αICAM-1), and RT plus anti-CD8 blocking (RT + αCD8) (n = 7–9 per group). Data are presented as mean ± SD. *, P <0.05; by 2-way ANOVA.

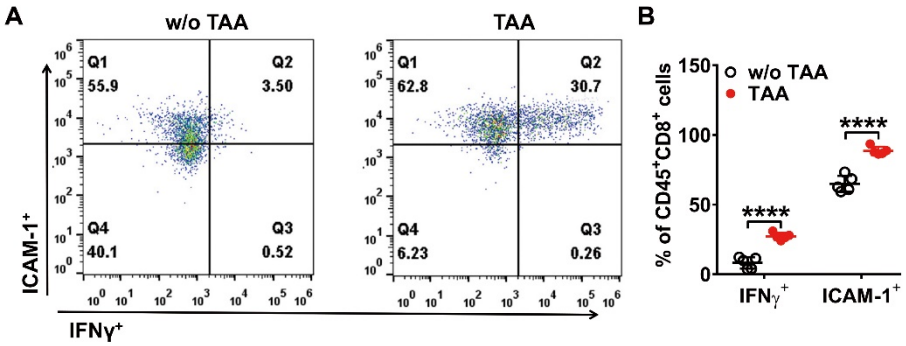

Figure S16. Expression analysis of IFNγ and ICAM-1 upon tumor-associated antigen (TAA) stimulation. (A–B) Representative flow cytometry plots (A) and quantitative analysis (B) of IFNγ and ICAM-1 expression of $CD8^+$ T cells after TAA stimulation (n = 5). Data are presented as mean ± SD. ****, P <0.0001; by unpaired Student t test.

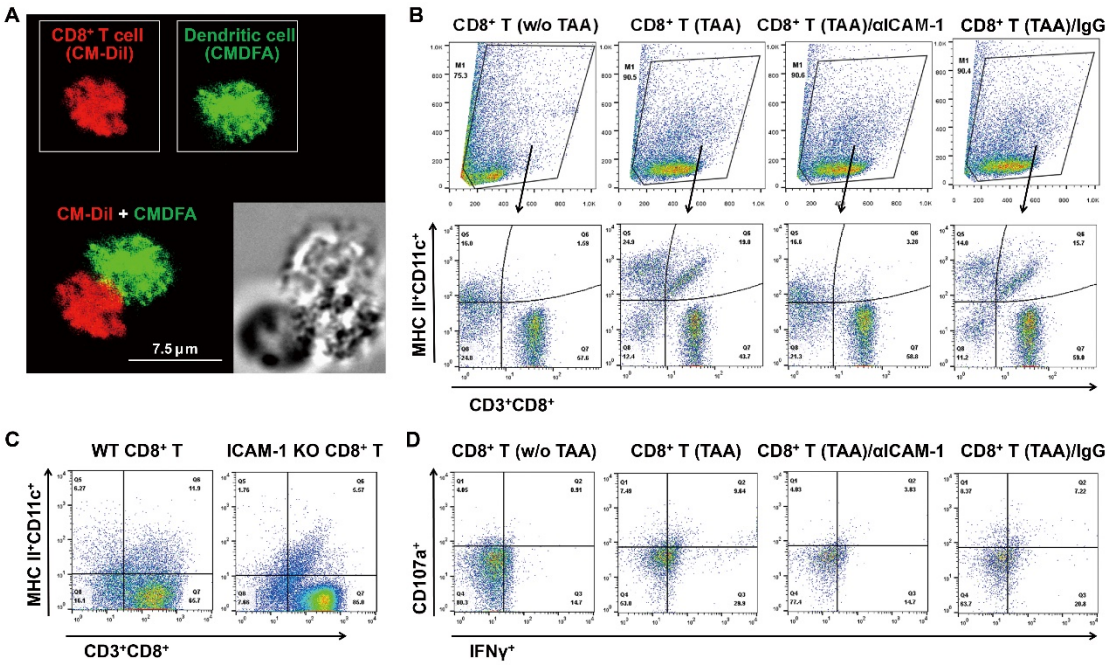

Figure S17. ICAM-1 blockade disturbs immune synapse formation between $CD8^+$ T cells and dendritic cells. (A–B) Representative confocal microscopy images (A) and flow cytometry plots (B) of mutual binding between $CD8^+$ T cells and dendritic cells blocked with anti-ICAM-1 antibody or isotype IgG control. (C) Flow cytometry plots of mutual binding between wild-type (WT) or ICAM-1 knockout (KO)-mouse-derived $CD8^+$ T cells and dendritic cells. (D) Representative flow cytometry plots of CD107a and IFNγ expression on $CD8^+$ T cells. TAA, tumor-associated antigen.

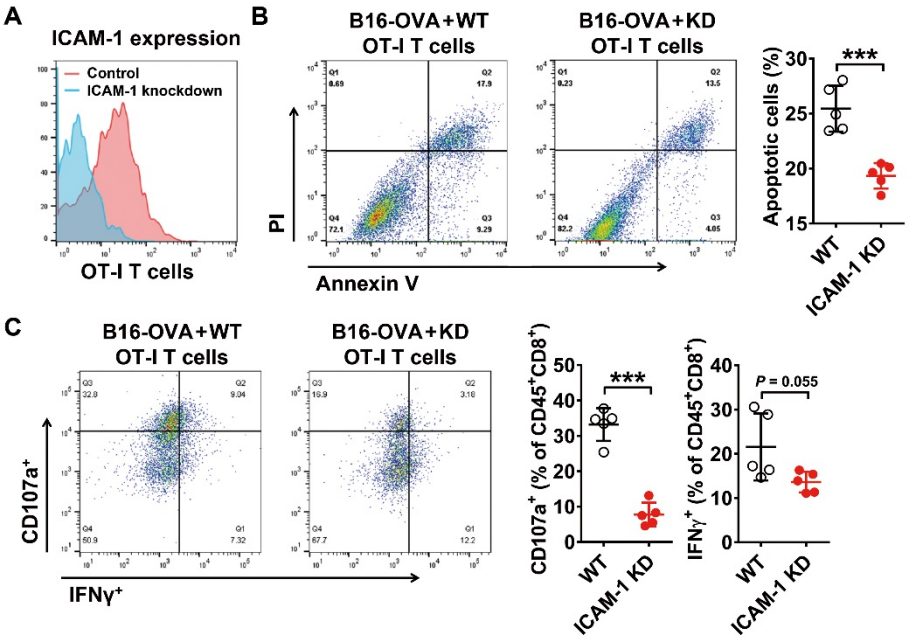

Figure S18. *In vitro* coculture study of ICAM-1 knockdown OT-I T cells and B16-OVA tumor cells. (A) ICAM-1 knockdown efficiency of OT-I $CD8^+$ T cell was confirmed by flow cytometry. (B–C) Control (WT) OT-I $CD8^+$ T cells or ICAM-1 knockdown (KD) OT-I $CD8^+$ T cells were cocultured with B16-OVA tumor cells in the presence of interleukin-2 for 2 days. Apoptosis of tumor cells (B) and activity of $CD8^+$ T cells (C) were analyzed by flow cytometric analysis. All the numerical data are presented as mean ± SD, n = 5. ***, P <0.001; by unpaired Student t test.

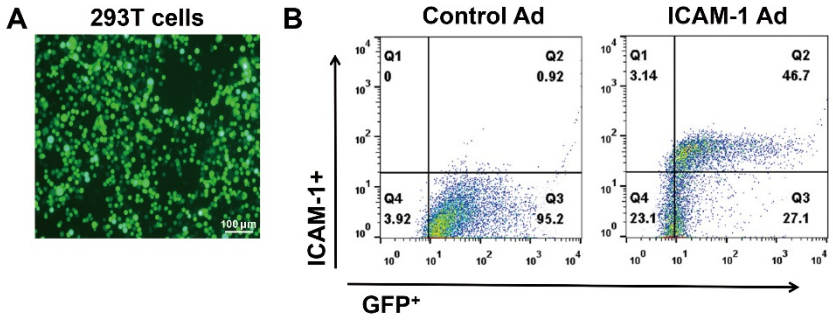

Figure S19. Transfection of ICAM-1 in 293T cells. (A–B) Transfection efficiency of ICAM-1 was determined by green fluorescent protein reporter protein detection using fluorescence microscopy imaging (A) and flow cytometry (B).

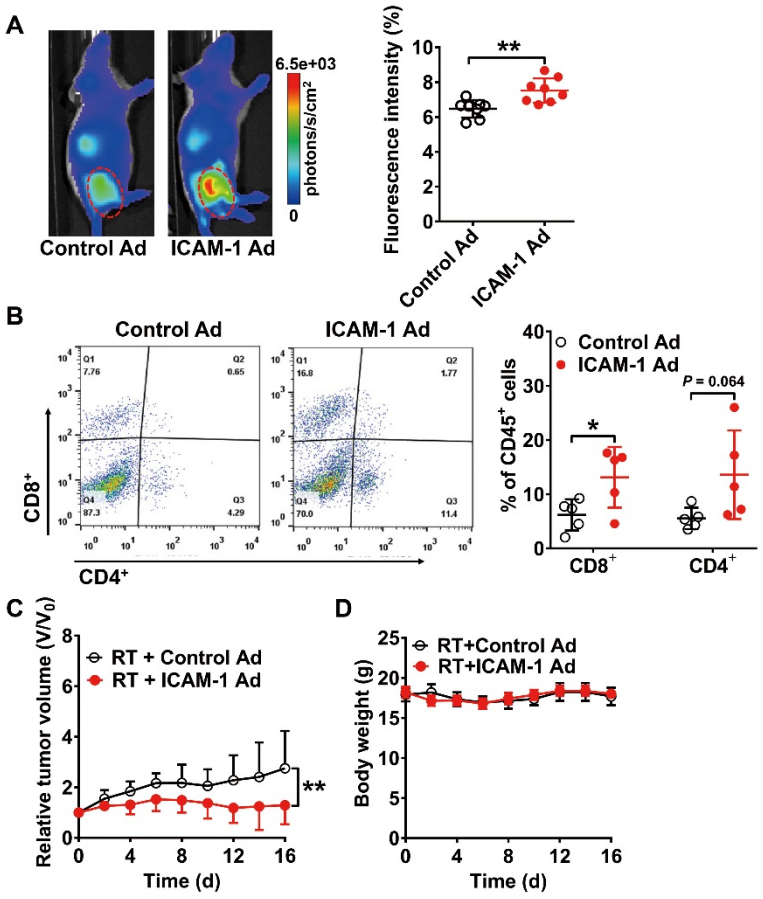

Figure S20. Effects of ICAM-1 Ad treatment in the 4T1 tumor-bearing mice. (A) Representative *in vivo* near-infrared fluorescence images and quantitative analysis of tumor uptake of Dye-αICAM-1/Fab at 6 h p.i. in 4T1 tumor-bearing mice with ICAM-1 Ad or control Ad treatment (n = 8 per group). Tumors are indicated by red circles. (B) Representative flow cytometry plots, and quantitative analysis of $CD8^+$ T cells and $CD4^+$ T cells in 4T1 tumors with ICAM-1 Ad or control Ad treatment (n = 5). (C–D) Tumor growth curves of irradiated tumor (C) and bodyweight (D) in 4T1 tumor-bearing mice after the indicated treatments: RT plus control Ad and RT plus ICAM-1 Ad (n = 9–10 per group). All the numerical data are presented as mean ± SD. *, P <0.05; **, P <0.01; by unpaired Student t test (A and B), or by 2-way ANOVA (C).

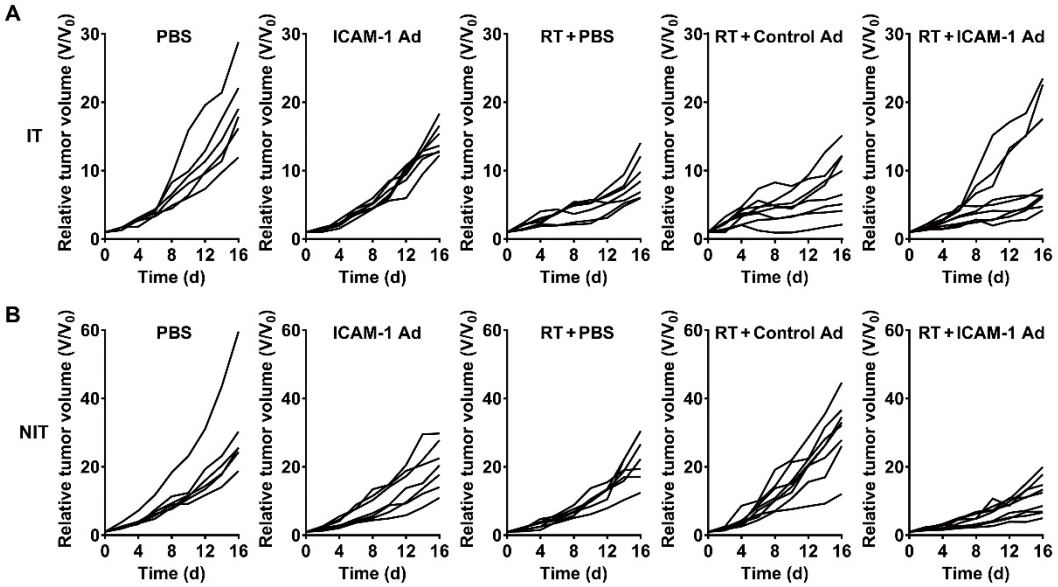

Figure S21. Tumor growth curves of 4T1 tumor-bearing mice after the combination of radiotherapy (RT) and ICAM-1 Ad treatment. (A–B) Individual growth curves of irradiated (IT) (A) and nonirradiated tumors (NIT) (B) in 4T1 tumor-bearing mice after PBS, ICAM-1 Ad, RT + PBS, RT + Control Ad, or RT + ICAM-1 Ad treatments. Average tumor growth curves of different groups are shown in Figure 4B of the main text.

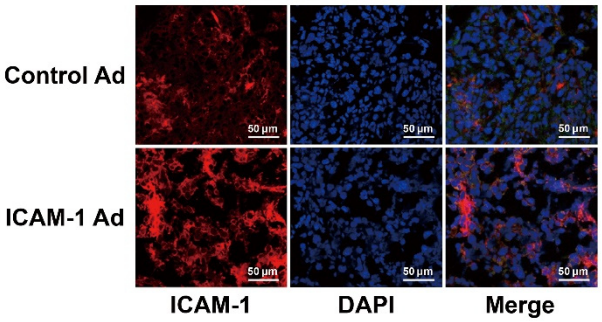

Figure S22. Immunofluorescence staining of ICAM-1 expression in the nonirradiated tumor tissues. Markedly higher expression of ICAM-1 was observed in the nonirradiated tumor tissues after treatment with radiotherapy (RT) plus ICAM-1 Ad than in those after treatment with RT plus control Ad.

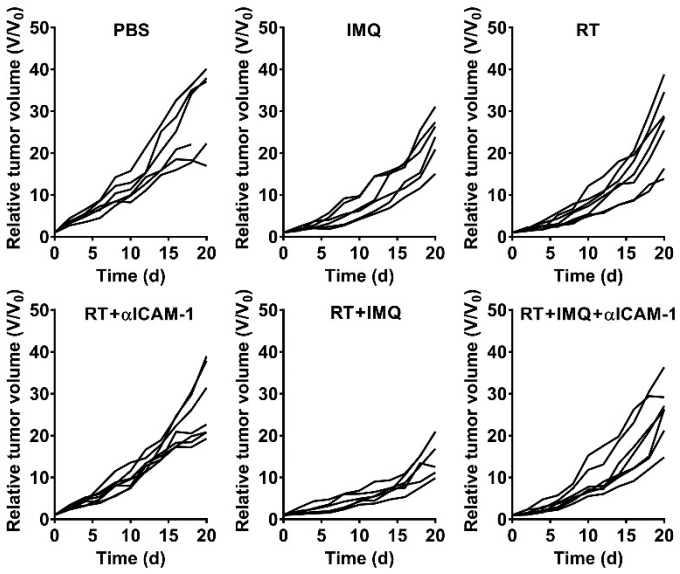

Figure S23. Tumor growth curves of 4T1 tumor-bearing mice after the combination of radiotherapy (RT) and IMQ treatment. Individual growth curves of nonirradiated tumors in 4T1 tumor-bearing mice after treatment with PBS, IMQ, RT alone, RT + αICAM-1, RT + IMQ, or RT + αICAM-1 + IMQ. Average tumor growth curves of different groups are shown in Figure 5E of the main text.

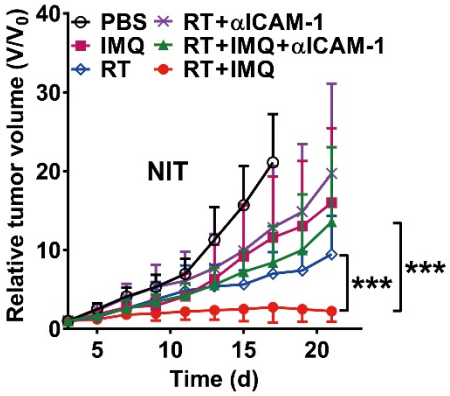

Figure S24. IMQ-induced ICAM-1 expression synergizes with local X-RT to inhibit nonirradiated tumor (NIT) growth in CT26 tumor-bearing mice. Tumor growth curves of NITs in CT26 tumor-bearing mice after the indicated treatments: control (PBS), IMQ alone, RT alone, RT plus anti-ICAM-1 blocking (RT + αICAM-1), RT plus IMQ plus anti-ICAM-1 blocking (RT + IMQ + αICAM-1), or RT plus IMQ (RT + IMQ) (n = 6–10 per group). Data are presented as mean ± SD. ***, P <0.001; by 2-way ANOVA.

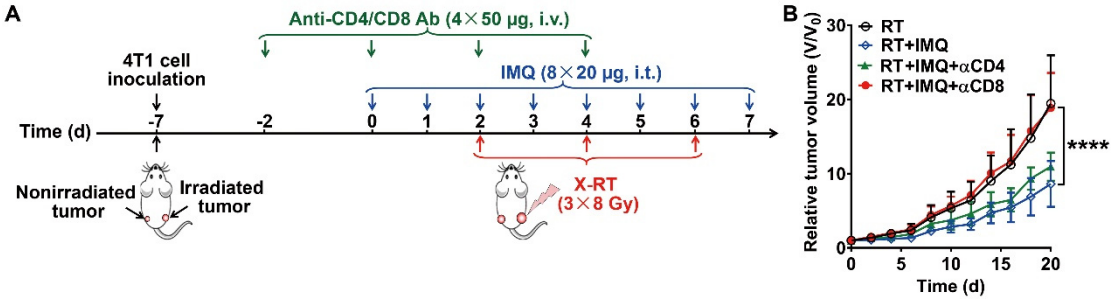

Figure S25. Depletion of $CD8^+$ T cells diminishes the abscopal effect of nonirradiated tumors induced by IMQ combined with X-RT in 4T1 tumor-bearing mice. (A) Schematic illustration of $CD8^+$ cells or $CD4^+$ cell depletion intervenes in local RT combined with IMQ treatment. (B) Tumor growth curves of nonirradiated tumors in 4T1 tumor-bearing mice after the indicated treatments: RT alone, RT plus IMQ (RT + IMQ), RT plus IMQ plus anti-CD8 blocking (RT + IMQ + αCD8), and RT plus IMQ plus anti-CD4 blocking (RT + IMQ + αCD4). Data are presented as mean ± SD. n = 8–12 per group. ****, P <0.0001; by 2-way ANOVA.

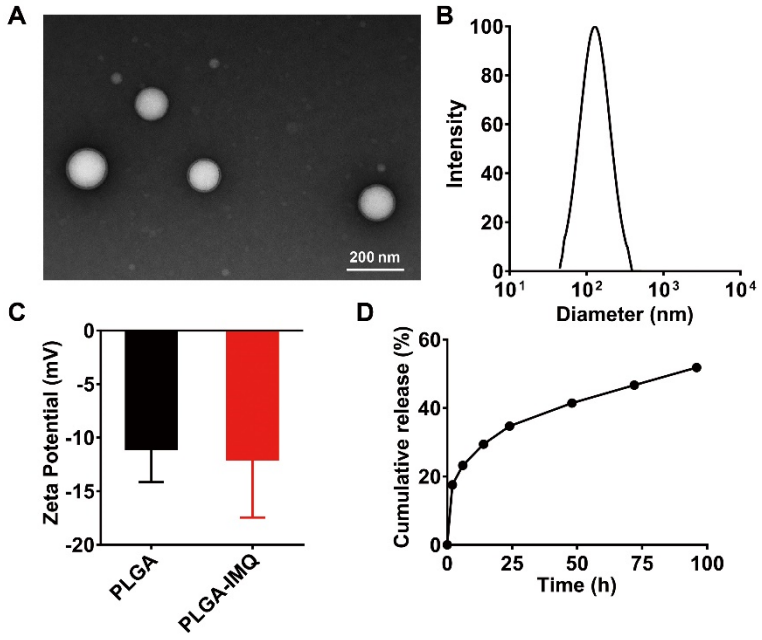

Figure S26. Characterization of PLGA-IMQ nanoparticles. (A) Transmission electron microscopy image of PLGA-IMQ nanoparticles. (B–C) Dynamic light scattering measurements of hydrodynamic size (B) and surface zeta potential (C) of PLGA-IMQ nanoparticles. (D) Time-dependent release profile of IMQ from PLGA-IMQ nanoparticles dispersed in PBS at 37°C. Data are presented as mean ± SD, n = 4. Note that the error bars in panel (D) are too small to be visualized.

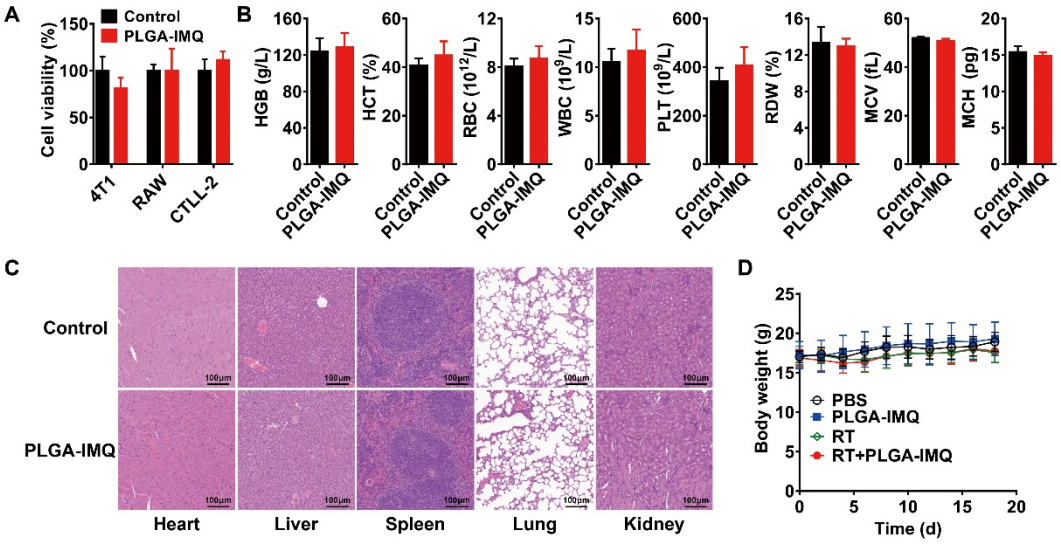

Figure S27. Toxicity study of PLGA-IMQ nanoparticles. (A) *In vitro* cell viability analysis of 4T1, RAW264.7, and CTLL-2 cell lines when treated with PBS control or PLGA-IMQ at a concentration of 720 μg IMQ equivalent/mL (n = 4 per group). (B) Blood samples were collected on day 12 after treatment with PBS control or PLGA-IMQ for the indicated analysis: hemoglobin (HGB), hematocrit (HCT), red blood cell (RBC), white blood cell (WBC), platelet (PLT), red cell distribution width (RDW), mean corpuscular volume (MCV), and mean corpuscular hemoglobin (MCH) (n = 5 per group). (C) Hematoxylin and eosin staining of major organs, including the heart, liver, spleen, lung, and kidney from mice treated with PBS control or PLGA-IMQ. (D) No significant body weight loss after treatment with PBS, PLGA-IMQ, RT alone, or RT + PLGA-IMQ in 4T1 tumor bearing mice was observed (n = 8 per group). All the numerical data are presented as mean ± SD.

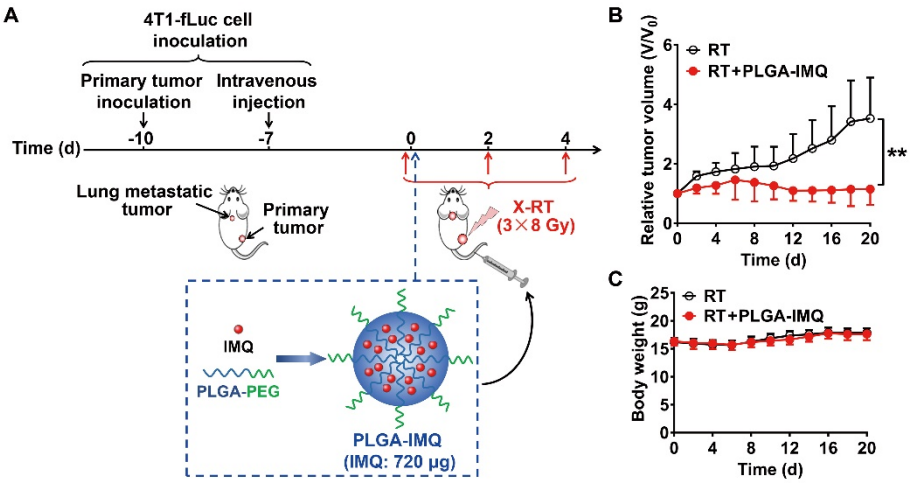

Figure S28. PLGA-IMQ enhances abscopal effect of local X-RT to eradicate established 4T1-fLuc lung metastatic tumors. (A) Schematic illustration of the schedule of X-RT combined with PLGA-IMQ treatment in a dual subcutaneous and lung metastatic 4T1-fLuc tumor model. (B) Tumor growth curves of the irradiated subcutaneous tumor after treatment with RT plus PBS or RT plus PLGA-IMQ. (C) All the treated mice showed no bodyweight loss. All the numerical data are presented as mean ± SD, n = 7–8 per group. **, P <0.01; by 2-way ANOVA. The growth of lung metastatic tumors was monitored by serial bioluminescence imaging as shown in Figure 6 F–G of the main text.

Table S1. Radiotherapy administrations and human tumor sample collection time points.

Patient #	Type of cancer	Gender	Age	RT dose	RT date	Sample collection date	
						before RT	after RT
1	Rectal cancer	Male	74	Rectal tumor: 50 Gy/25 f; Pelvic lymphatics: 45 Gy/25 f	01/05/2020-02/06/2020	12/31/2019	06/24/2020
2	Rectal cancer	Male	70	Rectal tumor: 56 Gy/25 f; Metastatic LNs: 62.50 Gy/25 f; Pelvic lymphatics: 50 Gy/25 f	11/11/2019-12/13/2019	11/04/2019	03/25/2020
3	Soft tissue sarcoma	Female	51	Tumor bed: 60 Gy/25 f; Low risk area: 50 Gy/25 f	03/18/2019-04/22/2019	01/25/2019	04/15/2019
4	Soft tissue sarcoma	Female	74	High risk area: 66 Gy/25 f; Recurrent tumor: 24 Gy/4 f; Low risk area: 50 Gy/25 f	04/12/2018-05/17/2018	02/26/2018	01/21/2019
5	Rectal cancer	Male	67	Tumor bed: 50 Gy/25 f; Metastatic LNs: 65 Gy/25 f; Preventive area: 50 Gy/25 f	03/31/2020-05/06/2020	08/08/2019	05/21/2020

Note: RT, radiotherapy; f, fractions; LNs, lymph nodes.

Table S2. Fluorescently labeled antibodies used in this study for flow cytometric analysis.

Reagent	Source	Identifier
Anti-mouse CD11a (PE)	Biolegend	Clone: M17/4; Cat#: 101107
Anti-mouse CD11b (APC)	Biolegend	Clone: M1/70; Cat#: 101212
Anti-mouse CD11c (PE-Cy7)	Biolegend	Clone: N418; Cat#: 117317
Anti-mouse ICAM-1 (PE)	eBioscience	Clone: YN1/1.7.4; Cat#: 12-0541-81
Anti-mouse ICAM-1 (FITC)	Prepared in-house	Not applicable
Anti-mouse CD3 (PE)	Biolegend	Clone: 17A2; Cat#: 100205
Anti-mouse CD3 (FITC)	Biolegend	Clone: 145-2C11; Cat#: 100305
Anti-mouse CD8 (FITC)	eBioscience	Clone: 53-6.7; Cat#: 11-0081-82
Anti-mouse CD8 (PE)	eBioscience	Clone: 53-6.7; Cat#: 12-0081-82
Anti-mouse CD4 (APC)	Biolegend	Clone: RM4-5; Cat#: 100516
Anti-mouse CD4 (PerCP-Cy5.5)	eBioscience	Clone: RM4-5; Cat#: 45-0042-82
Anti-mouse CD45 (AF700)	eBioscience	Clone: 30-F11; Cat#: 56-0451-82
Anti-mouse CD19 (PE)	Biolegend	Clone: HIB19; Cat#: 302207
Anti-mouse NK1.1 (APC)	eBioscience	Clone: PK136; Cat#: 17-5941-81
Anti-mouse IFNγ (APC)	Biolegend	Clone: XMG1.2; Cat#: 505809
Anti-mouse CD107a (PE-Cy7)	Biolegend	Clone: 1D4B; Cat#: 121619
Anti-mouse FoxP3 (PE-Cy7)	eBioscience	Clone: FJK-16s; Cat#: 25-5773-82
Anti-mouse MHCII (APC)	Biolegend	Clone: M5/114.15.2; Cat#:107614
Anti-mouse CD31 (PE-Cy7)	eBioscience	Clone: 390; Cat#: 25-0311-82

Dataset S1 (Microsoft Excel format; separate file)**.** List of identified proteins with altered expression levels (fold-change >2.5 compared to the control group) in different groups after radiotherapy.

SI References

1. Gao L*, et al.* (2016) Enhanced anti-tumor efficacy through a combination of integrin αvβ6-targeted photodynamic therapy and immune checkpoint inhibition. *Theranostics* 6(5):627-637.

2. Zhong L*, et al.* (2017) Quantitative proteomics reveals EVA1A-related proteins involved in neuronal differentiation. *Proteomics* 17(5):1600294

3. Zhao Y*, et al.* (2017) Chemotherapy-induced macrophage infiltration into tumors enhances nanographene-based photodynamic therapy. *Cancer Res* 77(21):6021-6032.

4. Lai J*, et al.* (2018) Noninvasive small-animal imaging of galectin-1 upregulation for predicting tumor resistance to radiotherapy. *Biomaterials* 158:1-9.

5. Feng X*, et al.* (2020) Clinical translation of a ^{68}Ga-labeled integrin alphavbeta6-targeting cyclic radiotracer for PET imaging of pancreatic cancer. *J Nucl Med* 61(10):1461-1467.

6. Liu Z, Jia B, Zhao H, Chen X, & Wang F (2011) Specific targeting of human integrin αvβ3 with ^{111}In-labeled Abegrin in nude mouse models. *Mol Imaging Biol* 13(1):112-120.